

Full length article

Crushing investigation of crash boxes filled with honeycomb and re-entrant (auxetic) lattices

Jonathan Simpson, Zafer Kazanci*

Advanced Composites Research Group, School of Mechanical and Aerospace Engineering, Queen's University Belfast, Belfast, BT9 5AH, United Kingdom



ARTICLE INFO

Keywords:

Auxetic
Crash box
Crashworthiness
Lattice structures
Quasi-static

ABSTRACT

This study investigates the crush response of lattice filled square tubes under quasi-static compressive loading. Auxetic lattice (auxetic strut and re-entrant) filled tubes have been compared to a non-auxetic (honeycomb) filled alternative and an empty tube. All structural lattices within this study were designed to be of equal mass. The experimental results were computationally validated using Abaqus®/Explicit. Experimental and numerical results show good agreement which highlights that the addition of lattice structures greatly improved the crashworthiness performance of the crash tube compared with an empty tube. By comparing the experimental values of energy absorption (EA), through the inclusion of a filler lattice a 62.6%, 64.0% and 79.1% increase over the empty tube were obtained for the auxetic strut, re-entrant and honeycomb structures respectively.

1. Introduction

Within the automotive industry, strict adherence to regulatory standards ensure the safety of all vehicles and passengers. With the demand for personal transportation increasing on a daily basis, there comes an inevitable increase in the number of collisions experienced. Of these, 1.3 million fatalities and 39 million injuries occur globally each year [1]. To improve performance, the design of vehicle safety systems must regularly evolve to ensure the highest protection capabilities. During a vehicle collision, the structure must be capable of absorbing kinetic energy from the crash and dissipate this in a controlled and irreversible manner. Crash boxes are broadly designed and employed for this exact purpose; to absorb and dissipate the direct impact force. Thin-walled energy absorbers have been reviewed and are described within the literature [1–5]. Crashworthiness may be defined as the “impact performance of a structure when it collides with another object” [6]. Therefore, the crashworthiness of a vehicle is of paramount importance within the preliminary design phase to ensure and uphold passenger safety.

Considerable research over the past several decades has been directed at improving the crashworthiness of structures subjected to impact, thereby reducing the injury to occupants. Thin-walled (TW) structures have been typically employed as energy-absorbing devices to enhance crashworthiness. A number of factors which typically influence their energy absorption capabilities including cross-sectional geometry,

base material and loading mode [1].

Numerous variations of tube geometry have been investigated numerically and experimentally over the years [7–11]. These profiles will fall into one or more of the following categories: hollow tubes, multi-cell tubes, tapered tubes (axially or transversely), nested tubes and filled tubes. To name a few from the studied literature, the most common profiles to analyse have been square [12], circular [13] and hexagonal [14] profiles. This can be explained by their availability, manufacturability and comparative ease to analyse.

There are many published research articles which have addressed the design issues and optimisation of crash tubes through variation of parameters such as wall thickness or cross-sectional profile. The correlative relationship between cross-sectional profile and crashworthy performance has been studied by many authors [15–19]. Additionally, significant research has been conducted regarding the selection of materials. This may be further subdivided into the TW tube material and the filler material. Currently, the most common materials for crash boxes and TW tubes include metallics, primarily dominated by aluminium and steel. Composite crash tubes [20–22], including carbon fibre and glass fibre reinforced plastics. Composites by design behave in an anisotropic manner. This can lead to difficulty when reproducing numerically and the manufacturing complexities. Conventional filler materials include lattice structures and foam materials, both of which have proven to provide a lightweight addition in providing enhanced performance experimentally and numerically [23].

* Corresponding author.

E-mail address: z.kazanci@qub.ac.uk (Z. Kazanci).<https://doi.org/10.1016/j.tws.2020.106676>

Received 2 July 2019; Received in revised form 10 February 2020; Accepted 11 February 2020

Available online 24 February 2020

0263-8231/© 2020 Elsevier Ltd. All rights reserved.

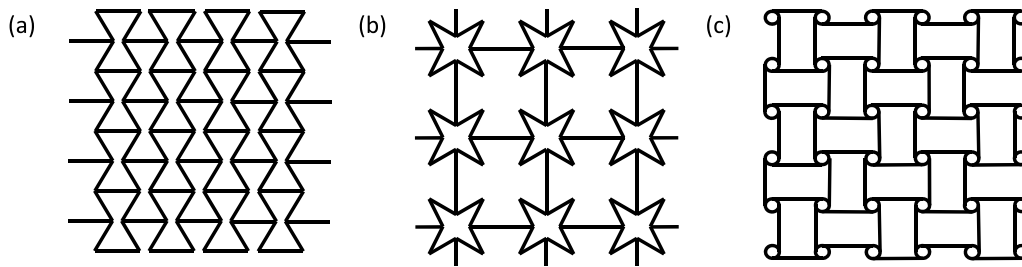


Fig. 1. Auxetic structural topologies (a) re-entrant (b) star and (c) anti-tetra-chiral.

These aforementioned studies focussing on appropriate material selection have all highlighted the energy absorption enhancement provided by convention materials, common to which is the positive Poisson’s ratio. However, materials and structures which exhibit a negative Poisson’s ratio (NPR) could be employed to further enhance the crashworthiness of these TW structures. NPR materials will contract transversely when axially compressed and will conversely expand transversely when expanded. These materials and structures are referred to as “auxetic”, a term first coined by Evans [24]. The theoretical existence of these NPR materials was first proposed by Love [25]. However, the prominence of research has only existed in the last three decades, following their formal discovery by Lakes [26]. Several auxetic topologies have been reported in the literature, with some of the most common architectures presented in Fig. 1.

The unique reaction under an applied force has been investigated in a few studies. Crash tube fillers have included auxetic foams [27,28] and auxetic lattices [29]. As a result, the full exploitation of the enhancements provided is relatively understudied. Additionally, research has focussed on auxetic foam and lattices under quasi-static [30,31] and dynamic [32,33] loading scenarios. These studies have generally focused on the microscopic and macroscopic behaviours, assessing the characteristics of auxetic geometries. However, this report will assess the performance of auxetic structures on the macroscopic scale filled in a crash tube.

This paper seeks to broaden the potential use of auxetic geometries within crashworthy automotive applications and assess the performance of macroscopic auxetic structural lattice filled crash tubes. An auxetic class of structures has been selected due to: their high porosity and large structural voids which results in a relatively small increase in overall mass [34]; auxetics are able to flow towards an area upon impact in a unique phenomenon referred to as “densification”, thereby increasing the overall hardness [35] and there is a significant increase in resilience

(especially under high strain rates, those typically experienced during a crash) [36]. These aforementioned material properties highlight the suitability of auxetics for use under crash scenarios.

The interaction among the crash tubes and filler structures plays an important role in enhancing the energy absorption behaviour of the structure. The majority of researchers working on filling the crush tubes with conventional foam or lattice structures. Auxetic foam and lattice types have only received limited attention despite their advantageous properties. Therefore, more investigations need to be conducted to understand the full potential of such materials. However, the numbers of studies on such foam and lattices have been limited making it worthwhile to be considered for further investigations.

The aim of this study is to investigate the crashworthiness performance of various auxetic and conventional lattices within TW crush tubes of square cross-sectional topology, under quasi-static compressive loading. An experimental study has been performed and is presented alongside a numerical study which provides potential finite element modelling techniques for the analysis of auxetic and non-auxetic filler structures within thin-walled tubes subjected to quasi-static compression.

2. Experimental methodology

2.1. Design and fabrication

2.1.1. Crash tubes

The main motivation of this study was to investigate and compare the energy-absorbing capabilities of an empty tube to that of one filled with structural lattices. Therefore, a commonly available square profile crush tube has been selected with the cross-sectional geometry of 50 × 50 mm, as presented in Fig. 2. A nominal wall thickness of 1.5 mm and overall tube length of 200 mm were selected. The selected tube material

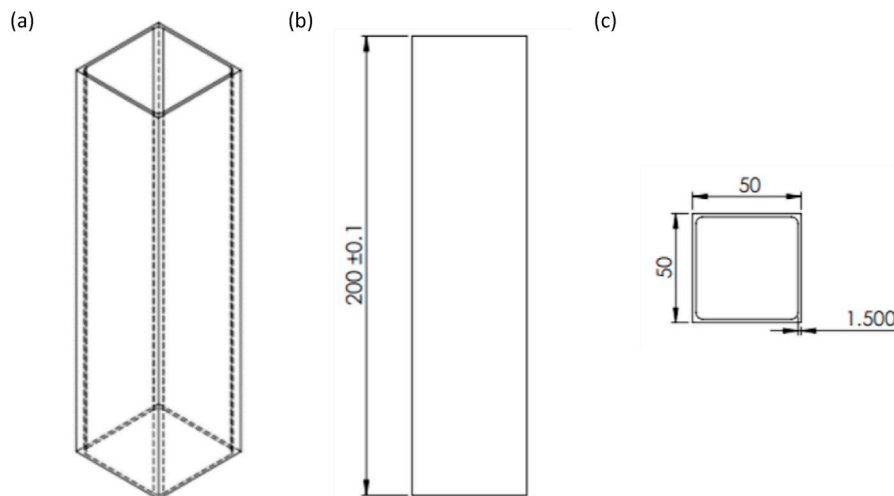


Fig. 2. Crush tube geometry: (a) isometric, (b) front and (c) top view (units in mm).

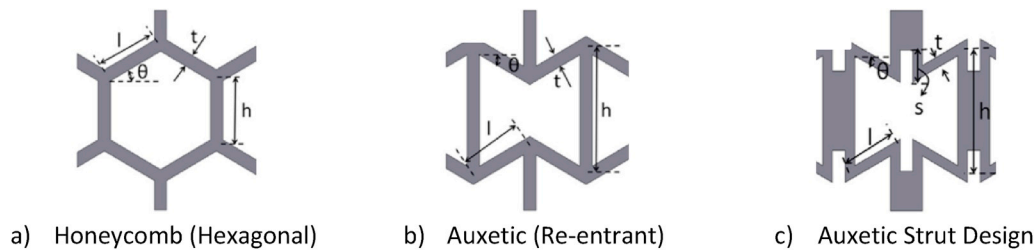
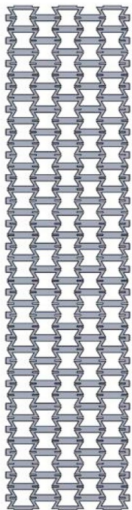
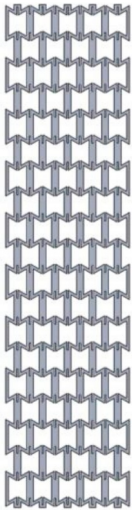
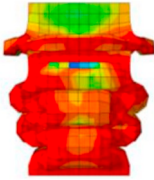
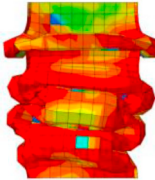


Fig. 3. Geometry configurations of respective designs analysed [38].



Fig. 4. Region of free space located at the top of each filled TW tube, highlighting the difference in the lattice and tube length.

Table 1
Comparison between differing lattice designs.

Parameter:	5 Cells Horizontal	5 Cells Vertical
Lattice Structure		
Deformed Crush Pattern		
Lattice Mass (grams)	195	195
Peak Crush Force (kN)	95.96	95.97
Mean Crush Force (kN)	65.18	66.07
Crush Force Efficiency (%)	68	69
SEA (kJ/kg)	7.11	7.97

is low-carbon steel manufactured in accordance with the BS EN 10305-5 standard [37].

2.1.2. Lattice fillers

Within the literature, the enhancements provided by using novel auxetic lattices have been identified. Therefore, three of the lattices presented in Ingrole et al. [38] have been selected as fillers for comparison against an empty crush tube. These three lattice geometries are presented in Fig. 3 and include the: (a) honeycomb, (b) re-entrant (c) auxetic strut as proposed by Ref. [38]. It should be noted that the fillers were manufactured 15–20 mm shorter than the TW tubes, as presented in Fig. 4. This would permit a void region at the top of each tube which could deform without initiating a large peak force. Common to both the re-entrant and auxetic-strut lattices is the NPR they induce under an applied force. However, both structures exhibit this behaviour when loaded in two directions: loaded horizontally and vertically. Therefore, several models, investigating auxetic cell orientation and unit cell size, were modelled using finite element package Abaqus®/Explicit [39]. It was found that the orientation of the lattice altered the performance, as is highlighted in Table 1. By using 5-unit cells vertically aligned, a 12.1% increase in Specific Energy Absorption (SEA) over horizontal alignment was observed. The inclined struts (l) deform easier than the straight struts (h), hence why the horizontal orientation absorbs less energy. Based upon the numerical results the geometry shown in Table 2 was finally selected. The (a) honeycomb (b) re-entrant and (c) auxetic-strut lattice structures (which were used as the crush tube fillers) have been presented in Fig. 5 - Fig. 6 and Fig. 7 respectively. These lattice structures were additively manufactured using a Stratasys Objet30 Pro 3D printer. This printer uses PolyJet technology and is capable of printing in detail up to 16-µm resolution. The material selected for the lattice structures was Vero Gray FullCure 850, the properties of which can be seen in Table 3, as provided by the manufacturer [40]. All specimen pre-test measurements can be seen in Table 4. In Fig. 8, the various filler lattice designs prior to crushing were demonstrated.

2.2. Experimental quasi-static compression tests

Quasi-static compression testing was conducted on the Zwick Roell Z100 universal test machine. The force-displacement data was recorded as the samples were crushed between two flat compression plates. A 100 kN load cell was used on all tested and compression was conducted at a constant rate of 5 mm/min, to ensure the quasi-static relationship was investigated. The samples were crushed to 60% displacement which corresponds to 120 mm of vertical travel.

2.3. Performance indicators

Different parameters are used to compare the performance and crashworthiness of various energy absorbing devices. The indicators used within this study include Initial Peak Force (P_{max}); Energy Absorption (EA); Specific Energy Absorption (SEA); Mean Crush Force (MCF) and Crush Force Efficiency (CFE).

The peak force is the force required to initiate plastic deformation within the tube and hence begin the energy absorption. Total energy

Table 2
Geometric parameters of lattice structures.

Unit Cell Topology	h (mm)	l (mm)	t (mm)	s (mm)	θ (°)	ρ^*/ρ_s	ν_y^*
(a) Honeycomb	5.00	5.00	1.77	n/a	30	0.4088	1.0000
(b) Re-entrant	10.50	5.01	1.38	n/a	-30	0.4082	-1.0639
(c) Auxetic Strut	11.00	3.45	1.00	3.00	-30	0.3381	-0.6329

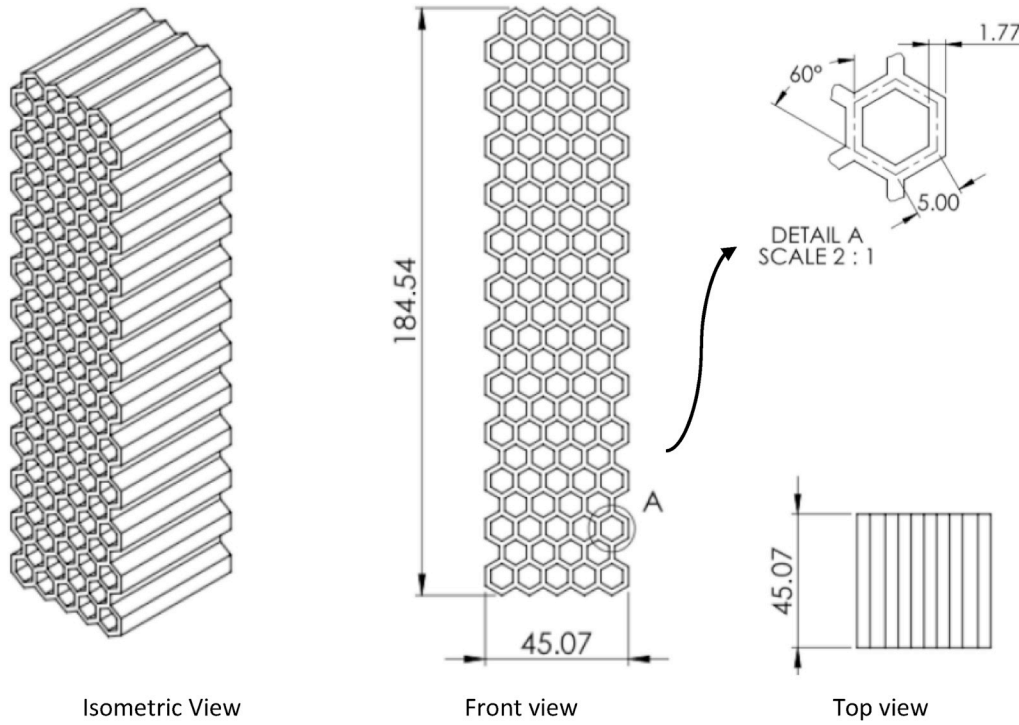


Fig. 5. Honeycomb (entrant) lattice geometry (units in mm).

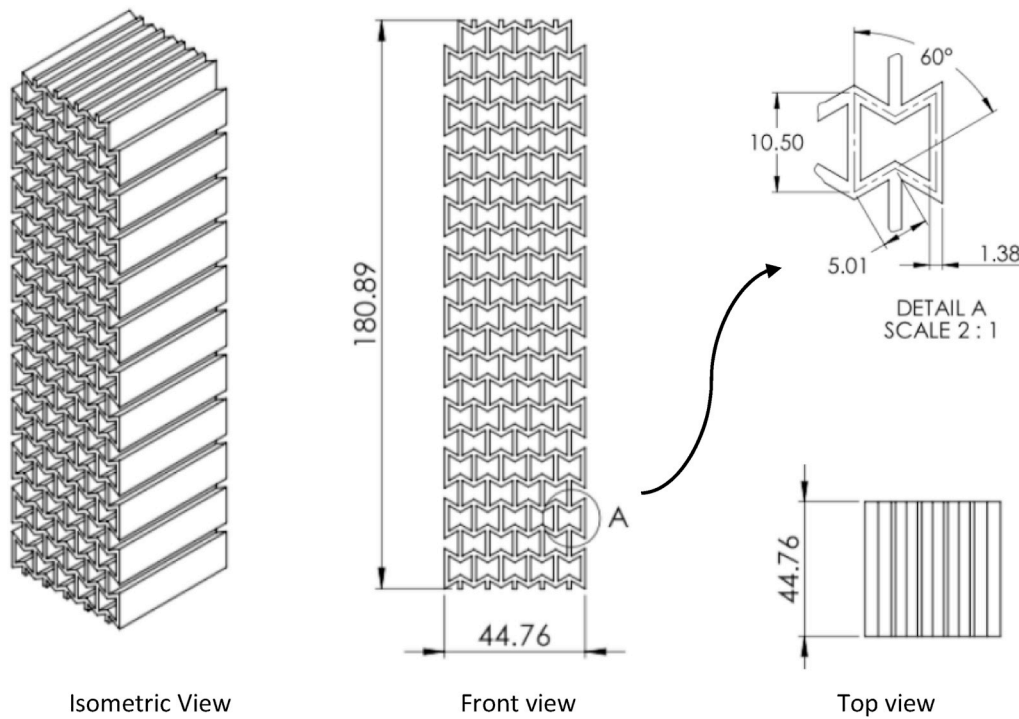


Fig. 6. Auxetic (re-entrant) lattice geometry (units in mm).

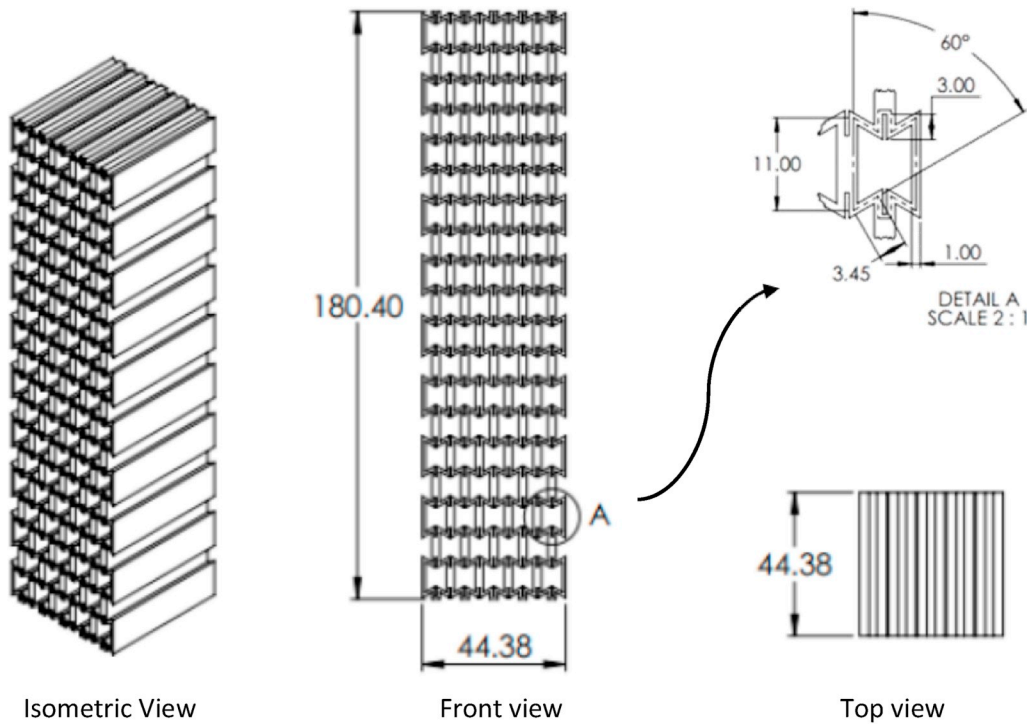


Fig. 7. Auxetic strut lattice geometry (units in mm).

Table 3
Material properties of Vero Gray FullCure 850 [40].

Property	Value	Units	ASTM
Tensile strength	50–65	MPa	D-638-03
Elongation at break	10–25	%	D-638-05
Modulus of Elasticity	2000–3000	MPa	D-638-04
Flexural Strength	75–110	MPa	D-790-03
Flexural Modulus	2200–3200	MPa	D-790-04
Polymerized Density	1170–1180	kg/m ³	D792

absorption through plastic deformation is calculated as the area under the force-displacement curve, using Eq. (1):

$$EA(d) = \int_0^d P(\delta)d\delta \quad (1)$$

where d is the total crushing distance, P is crushing force and δ is the instantaneous crush displacement.

Given that mass is a key indicator in any automotive structural design, specific energy absorption provides an indicator of the energy absorbed per unit mass, as presented in Eq. (2). A high EA and SEA are highly desirable within crashworthy applications.

Table 4
Measurements of each tube and lattice tested.

Filler Geometry	Cross-sectional Area (mm ²)		Tube Height (mm)	Lattice Height (mm)	Tube Thickness (mm)	Tube Mass (grams)	Lattice Mass (grams)	Overall Mass (grams)
	Tube	Lattice						
Empty	2540.64	–	200	–	1.51	425	–	425
	2533.55	–	200	–	1.48	425	–	425
	2527.49	–	200	–	1.49	428	–	428
Honeycomb	2535.07	2036.72	200	185	1.47	426	166	592
	2526.52	2036.71	200	185	1.50	426	166	592
Re-entrant	2529.04	2007.49	200	181	1.51	428	167	595
	2539.14	2007.94	200	181	1.48	428	167	595
Auxetic Strut	2528.56	1974.02	200	180	1.50	425	169	594
	2537.12	1972.25	200	180	1.50	427	169	596

$$SEA = \frac{EA}{m} \quad (2)$$

where m is the structural mass.

Mean crush force is based upon this absorbed energy at a particular displacement and is calculated using Eq. (3):

$$MCF = \frac{EA}{\delta} \quad (3)$$

Finally, crush force efficiency states the uniformity of the force-displacement curve and is presented as the percentage of mean crush force to peak crush force, as presented by Eq. (4):

$$CFE = \frac{MCF}{P_{max}} \times 100 \quad (4)$$

This value is commonly presented as a percentage value and a CFE of 100% implies ideal and uniform energy absorption has occurred.

3. Numerical modelling

Finite Element (FE) models were constructed using Abaqus®/CAE 2017 [38] software. Within this, Abaqus®/Explicit models were created

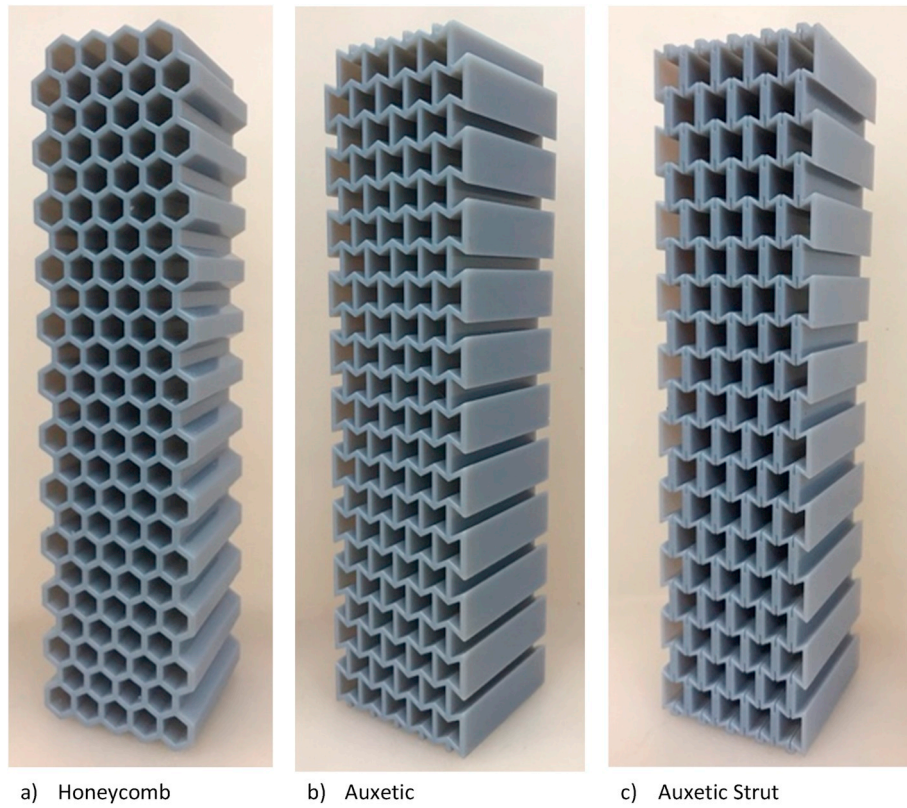


Fig. 8. 3D printed lattices.

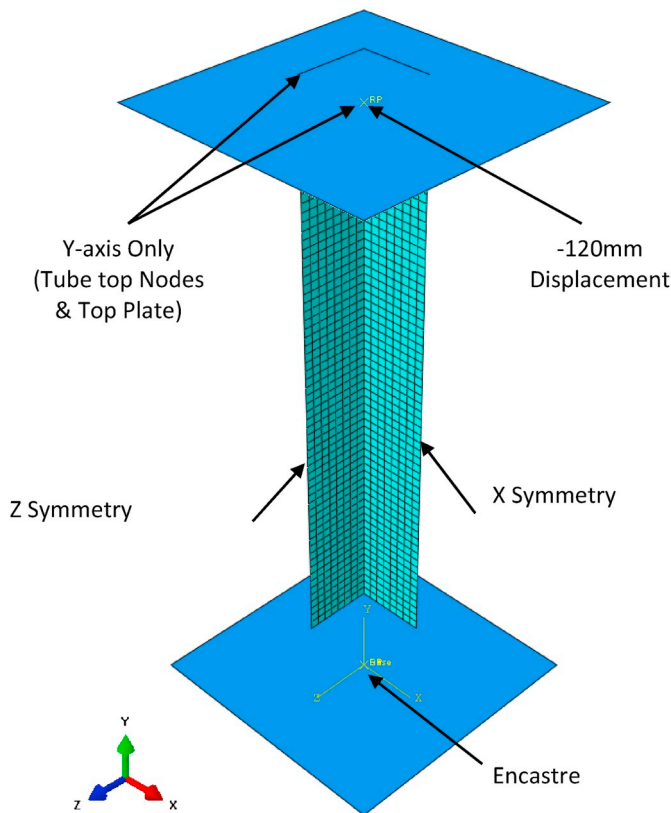


Fig. 9. Boundary conditions applied within Abaqus®/Explicit.

as they are ideally suited to non-linear, transient scenarios such as the slow crushing of an energy absorbing device.

As the geometry of the empty tube is symmetric a quarter model of the specimen was modelled. Quadrilateral shell elements with four nodes (S4R) and five integration points through the thickness were utilised. The geometry of the tube was as stated in Fig. 2. The material properties of the mild steel within this study are $E = 200 \text{ GPa}$, $\rho = 7132 \text{ kg/m}^3$, $\sigma_y = 265 \text{ MPa}$ and $\nu = 0.28$. The post-yield stress-strain data used in the FE analysis was taken from Seitzberger et al. [41] who conducted tensile tests on cold rolled mild steel specimens. A power-law relationship was further incorporated; with Bulk Modulus (K) = 565 MPa and $n = 0.192$.

The boundary conditions for the empty tube model are shown in Fig. 9. By applying symmetry to the two vertical edges of the tube movement in the z and x-direction was prohibited and potential slippage was avoided. The displacement was applied using the tabular amplitude function. Where initial displacement was 0 mm and the final displacement was 120 mm. This ensured the plate moved with a constant velocity and would best replicate the experimental control function. A friction coefficient of 0.2 was applied to the whole model. General contact was also employed to prevent any penetration between surfaces. Each simulation used a step time of 3 s. However, mass-scaling was applied to the whole model every increment, with a target time of $1.25 \times 10^{-5} \text{ s}$. Mass-scaling was utilised due to the quasi-static nature of the simulation.

For the tubes filled with a lattice structure, a full model was created i. e. not a quarter model simplification as shown in Fig. 10. This was to ensure that the correct deformation pattern throughout the lattice was identified. As discovered by Ingrole et al. [38] deformation did not occur in a symmetric manner in free space. It was, therefore, assumed the same would be true for the confined lattice. The boundary conditions were as shown in Fig. 9, with the removal of the x- and z-symmetric boundary conditions. An additional constraint tying the tube base nodes to the rigid base was introduced to compensate for the removal of symmetry

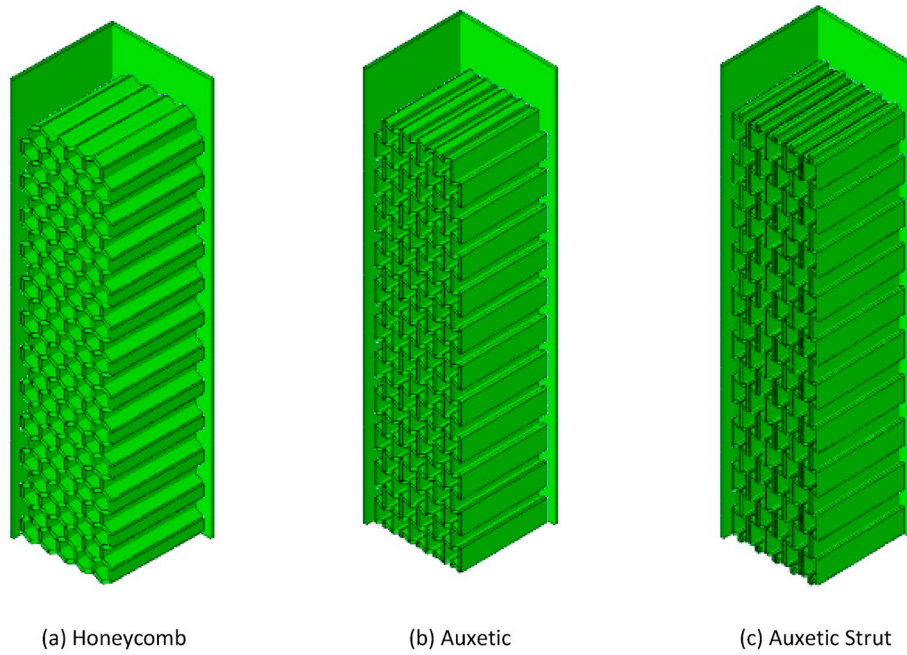


Fig. 10. Abaqus models showing cutaway square tube sections with lattice structures.

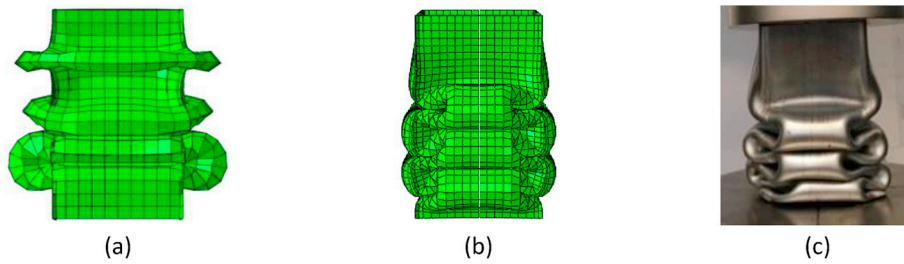


Fig. 11. Comparison of the deformation of the empty TW tube with the computational model: (a) geometric perfection, (b) an included imperfection, (c) experimental folding pattern.

($u_1 = u_2 = u_3 = 0$). The same mild steel material properties as stated previously were utilised. For the lattice, the parameters used were $E = 2$ GPa, $\rho = 1175$ kg/m³, $\sigma_y = 50$ MPa and $\nu = 0.35$. No post yielding behaviour for the lattice was included, due to the brittle nature of the material.

The experimental data obtained for the quasi-static crushing enabled a direct comparison and validation of the developed FE model. Mesh convergence was conducted in order to ensure the simulation presented an accurate representation of the experimental results. The force-displacement graphs were compared each time as the mesh was refined. Global seed size of 3.5 was selected which allowed the simulation to run without excessive mesh distortion.

The FE model assumed a perfectly straight tube with perfect dimensional characteristics; however, the experimental specimens were irregular and not identical. Therefore, during initial simulation development, the folds observed within the tube were ununiform, as presented in Fig. 11 (a).

To overcome and more accurately represent the experimental crushing pattern observed, an ‘imperfection’ was introduced to the model. In the present study, a linear perturbation buckling model was created. This buckle function within Abaqus®/Explicit allows the user to determine the natural buckling modes which could occur within the structure. For the present study, only the first 20 modes were considered. It was found that the 18th mode was most similar to the actual failure of the structure during experimental testing. These modes are then given a scaling factor within the Abaqus®/Explicit input file.

Fig. 11 (b) highlights the benefits of applying this two-step procedure and the obvious improvement in results.

4. Results and discussion

4.1. Deformation behaviour

Another key measurable output from both the FE simulations and experimental work is the deformation patterns of the TW tube. By having a uniform folding pattern, the energy is absorbed by the structure in a controlled manner. A comparison between the deformation patterns observed experimentally and obtained computationally through the FE simulations has been made for each of the tubes and filler combinations tested. Additionally, the force-displacement curves for each TW tube have been presented.

4.1.1. Empty TW tube

Table 5 presents the experimental and FE deformation patterns of the empty tube at an identical 40 mm sequential displacements increasing from 0 mm (start location) to 120 mm (full compression). As presented, the experimental and computational deformation modes compare well. Initially, the folds develop from the lower fixed compression plate with three distinct folds developing progressively upwards during the compression.

The corresponding experimental and numerical force-displacement curves for the empty tube is presented in Fig. 12. Each distinct peak

Table 5
Comparison of experiment & FEA fold patterns on an empty tube.

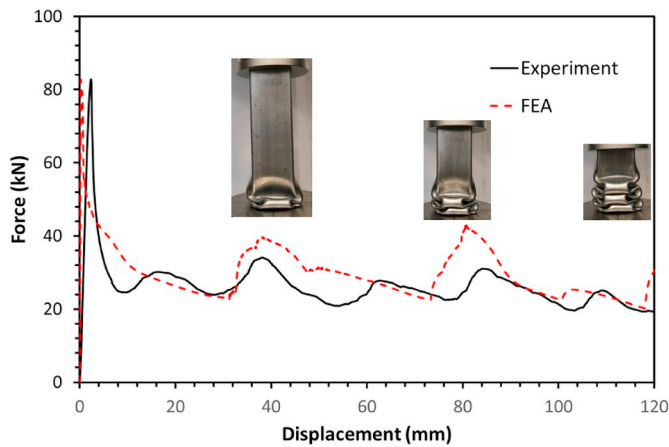
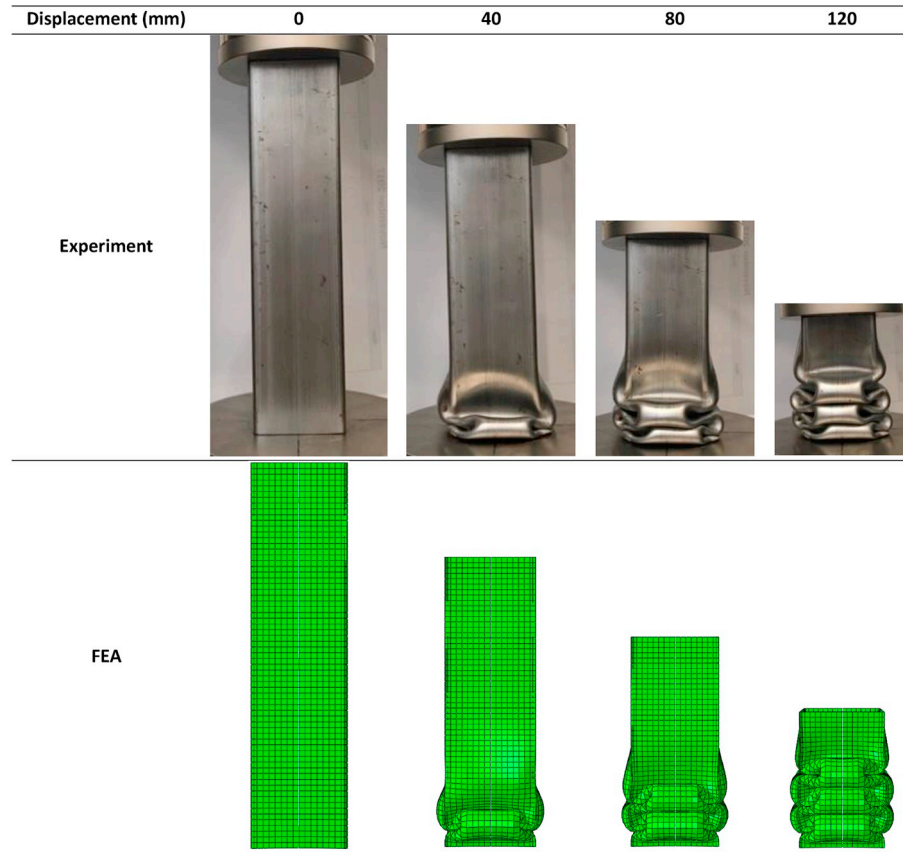


Fig. 12. Comparison of experiment & FEA force-displacement curves for empty tube (with deformation patterns at 40, 80 & 120 mm).

on the curve corresponds to a new fold forming within the structure. Good agreement between the experimental and numerical data is clearly displayed. Any discrepancy between the results is due to the initial flaws contained within the manufactured samples. One possible explanation could be the method selected for cutting the square tubes to the desired 200 mm length. A circular saw was selected and therefore the top tube surface was not machined to ensure a flat surface. This can cause only one edge of the tube to be in contact with the compression plate. Additionally, other flaws within the tubes could include tube straightness and the internal radii not being modelled within numerical

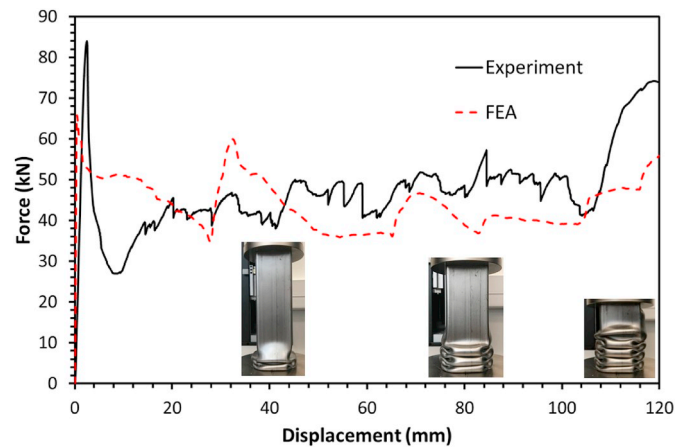


Fig. 13. Comparison of experiment & FEA force-displacement curves for honeycomb filled tube (with deformation patterns at 40, 80 & 120 mm).





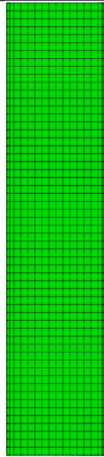
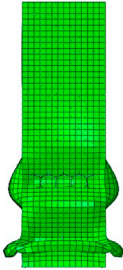
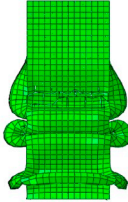
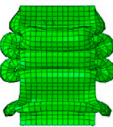
simulations. However, by calculating the area under each curve and obtaining the total energy absorbed, there was only a 12.2% error between the averaged experimental and numerical results.

The initial peak force magnitude of both the numerical and experimental simulation compare very well with only a 1.0% difference obtained. The numerical results, however, predict this peak sooner than the experimental test because of the universal test machine compliance.

4.1.2. Honeycomb (hexagonal) filled TW tube

The corresponding experimental and numerical force-displacement

Table 6
Comparison of experiment & FEA fold patterns on a honeycomb filled tube.

Displacement (mm)	0	40	80	120
Experiment				
FEA				

curves for the honeycomb filled tube is presented in Fig. 13. For both experimental specimens filled with a honeycomb lattice, the structure initially failed at the bottom surface, as shown in Table 6. This failure method did not match the results obtained for the auxetic strut and re-entrant designs, which progressively failed from the top surface.

Another major difference between honeycomb and other specimens tested is that five energy dissipating folds were formed. This additional fold is another reason why the EA and SEA of the honeycomb structure are superior to the auxetic geometries analysed.

The honeycomb structure was capable of providing the greatest EA and SEA of the tested specimens. Here, the honeycomb structure provided a 79.1% increase in EA and a 28.9% increase in SEA over the empty tube. The reason for this is in part due to the unit cell topology. While auxetic unit cells make use of internal structural cell walls to provide their counter-intuitive behaviour, non-auxetic cells (honeycomb) have no internal cell walls. All structural lattices within this study were designed to be of equal mass, and as a result, the three different unit cells have different wall thicknesses. The honeycomb structures have the largest thickness of 1.77 mm and so provide additional stiffness in the direction of loading.

4.1.3. Re-entrant filled TW tube

For the re-entrant filled tube, unlike the honeycomb filled tube, the first fold initiated at the top of the compression tube and formed sequentially vertically downwards, as shown in Table 7. The experimental and numerical results for force-displacement are presented in

Fig. 14. The results obtained by the finite element model and experimental study are distinctly different. The finite element model has relatively poor results, especially at the densification regions. In reality the self-contact mechanism is very complex, and deviation occurs in the progressive deformations. For this reason, the densification region of the numerical model is not fully compatible with the experimental results. Here it can be observed the much greater drop in force when the lattice struts are broken when compared with the auxetic strut (Fig. 17). This substantiates the findings within Ingrole et al. [38] who suggested there are stress concentrations formed within the re-entrant lattice causing more brittle behaviour. It was proposed by Ref. [38] that the auxetic-strut topology would reduce this phenomenon as sharp variations in force are not ideal for occupants of the vehicle during a crushing scenario.

When the re-entrant filled tubes were crushed the folding pattern was less repeatable. Of the two specimens tested experimentally, one failed at the top whereas the other initiated at the bottom. The final lobe on the specimen was much less rounded, and the lobes did not come into contact. The physical width of the lobe was also noticeably larger than the previous folds, as highlighted in Fig. 15.

Again, for the re-entrant filled tube, a releasing of the stored energy caused the TW tube to move upwards on the removal of the load. Despite the sharp changes in force, the re-entrant structure provided a 2.02 kJ increase in energy absorption over the empty tube. This leads to a 17.4% increase in SEA over the empty tube.

Table 7
Comparison of experiment & FEA fold patterns on a re-entrant filled tube.

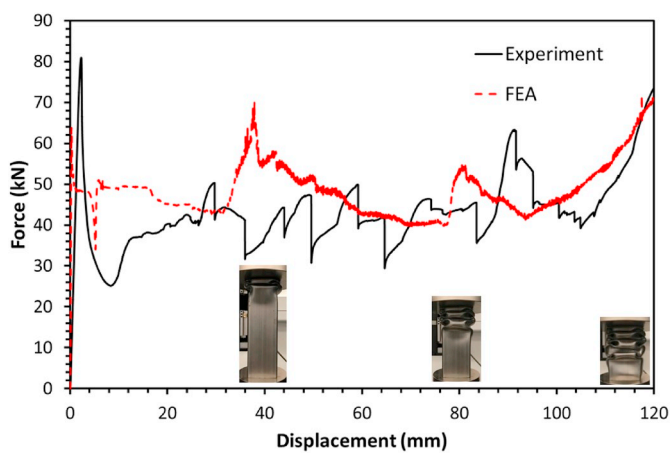
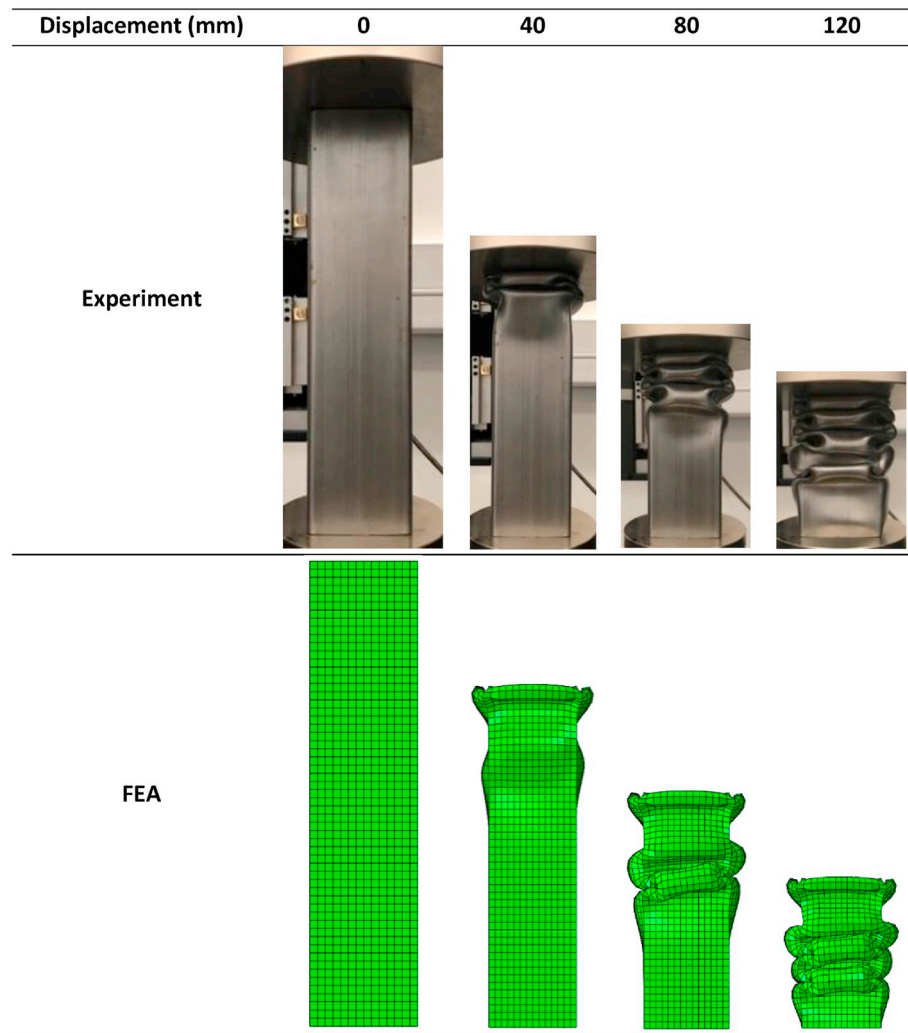


Fig. 14. Comparison of experiment & FEA force-displacement curves for re-entrant filled tube (with deformation patterns at 40, 80 & 120 mm).

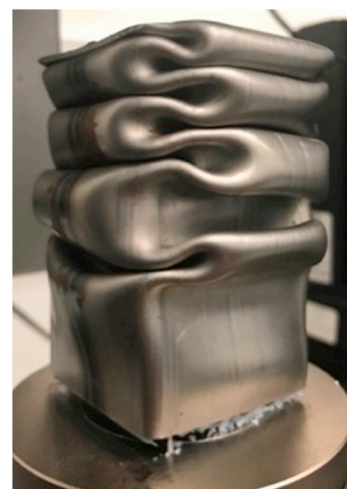


Fig. 15. Irregular fold on re-entrant filled tube.

Table 8
Comparison of experiment & FEA fold patterns on an auxetic strut filled tube.

Displacement (mm)	0	40	80	120
Experiment				
FEA				



Fig. 16. Lattice protruding from tube.

4.1.4. Auxetic strut filled TW tube

By including the auxetic strut within the TW tube, the deformation patterns observed are presented in Table 8. Conversely to the empty tube which formed at the bottom, the first deformation fold occurs at the top of the tube where the compression plate is vertically displaced. This is due to the empty space available at the top of the tube, as shown in Fig. 4. It was vital to ensure that global buckling did not occur as only a progressive stable collapse leads to high energy absorption. By designing the lattices to be shorter than the tube it guaranteed the top section had the least material across the cross-sectional area and therefore ensured the deformation was repeatedly initiated from there.

Once the experimental test was completed and the top plate moved up to the start position it could be seen that the auxetic lattice began to immediately move out of the undeformed end of the tube, as shown in

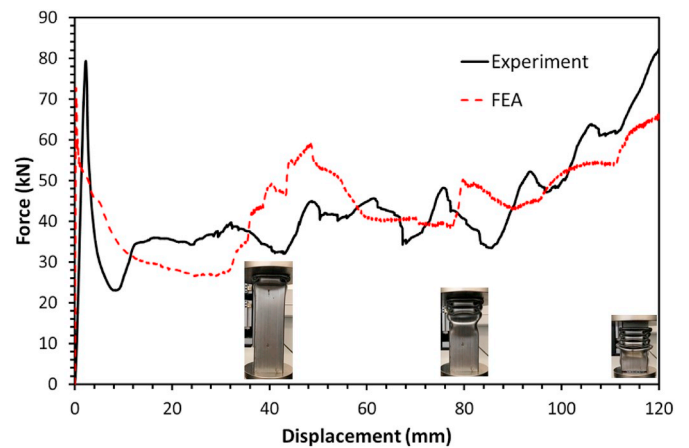
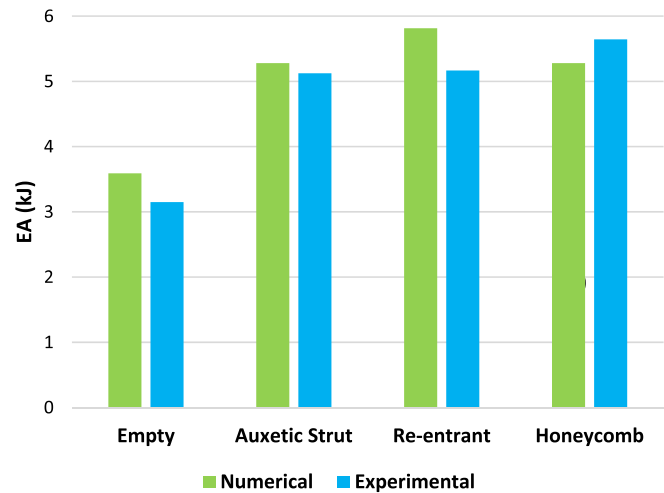


Fig. 17. Comparison of experiment & FEA force-displacement curves for auxetic strut filled tube (with deformation patterns at 40, 80 & 120 mm).

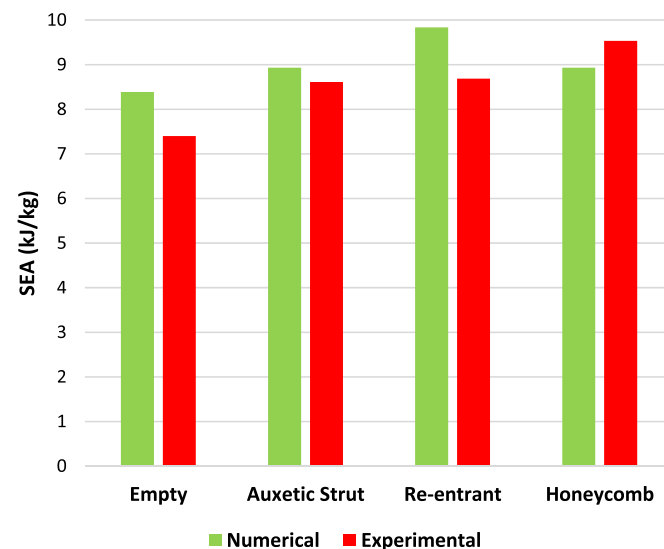
Fig. 16, eventually lifting the tube completely off the base support. This shows that the lattice structure had densified significantly during the test to absorb the energy. This stored energy is then released when the load is removed. The steady increase in peak amplitude, from 90 mm displacement onwards, also shows that the lattice is densifying and a continually increasing force is required to create a new fold in the sample. Experimentally, the crushing force was higher than the initial

Table 9
Properties obtained from experimental compression tests.

Sample Description	Mass (kg)	P_{max} (kN)	MCF (kN)	CFE (%)	EA (kJ)	SEA (kJ/kg)
Empty	1	0.425	82.78	29.04	35.08	3.49
	2	0.425	84.03	25.32	30.13	3.04
	3	0.428	83.56	24.41	29.22	2.93
Honeycomb	1	0.592	84.08	47.66	56.69	5.72
	2	0.592	83.93	46.40	55.29	5.57
Re-entrant	1	0.595	80.91	43.19	53.38	5.18
	2	0.595	81.15	42.93	52.90	5.15
Auxetic Strut	1	0.594	85.40	42.95	50.29	5.15
	2	0.596	80.92	42.44	52.45	5.09



(a)



(b)

Fig. 18. Comparison between all models for (a) energy absorption and (b) specific energy absorption.

peak force from 118.5 to 120 mm. This scenario should be avoided for passenger safety and further work should be conducted on the FE model to replicate this result.

A distinct difference between the empty and filled tube is the number of folds formed during deformation. The auxetic strut lattice filled tube produced four distinct folds during the 120 mm crush, as opposed to the empty tube which produced three. The folds are also more compact within the filled tubes due to the limited space available when a filler structure is included. The force-displacement curves for the numerical and experimental auxetic strut filled tubes are presented in Fig. 17. Again, the number of peaks observed corresponds to the formation of each fold. The deformation pattern obtained is symmetric in nature and therefore controlled, as is desirable for energy absorbing devices. Through the formation of an additional fold and the densification and crush of the filler structure, the auxetic strut filled TW tube was capable of absorbing 5.12 kJ of energy, a 62.6% increase over the empty tube. Additionally, despite the increased mass of 0.59 kg, the auxetic strut filled tube was capable of providing a 16.4% increase in SEA of 8.61 kJ/kg compared with the 7.40 kJ/kg of the empty tube.

4.2. Performance indicators

The experimental percentage crush and corresponding reaction force were generated from the test machine. Using this data, the performance indicators outlined in Section 2.3 were calculated and are presented in Table 9. The experimental values of energy absorption and specific energy absorption have been averaged and are presented in Fig. 18, alongside the results obtained from computational modelling.

From Fig. 18, it may be observed that both EA and SEA increase by using a lattice filled tube. By comparing the experimental values of energy absorption, through the inclusion of a filler lattice a 62.6%, 64.0% and 79.1% increase over the empty tube may be obtained for the auxetic strut, re-entrant and honeycomb structures respectively. This corresponds to a 16.4%, 17.4% and 28.9% increase in SEA. By comparing the thickness of each vertical strut, it may be observed that the honeycomb (hexagonal) structure with a cell wall thickness of 1.77 mm provides the greatest SEA enhancement. The re-entrant and auxetic strut lattices both featured thinner vertical cell walls and hence observed a lower EA for an equivalent mass. All three structures, however, provided an improvement over the empty tube. This improvement was obtained through the brittle fracture of the filler structures which crush in addition to the plastically deforming tube. The experimental and numerical values obtained compare well for the EA and SEA.

Across all experimental tests, the peak force obtained was 82.5 kN ± 1.5 kN, which is characteristic of mild steel and is unaffected regardless of whether the tube was filled or unfilled. This constant value of P_{max} is due to the difference in height between the filler and tube, as shown in Fig. 4. This height differential means the MCF, CFE, EA and SEA can all be increased with no impact on the P_{max} . When applied to a crash situation it is important not to increase the initial force (P_{max}) the passengers' experience, as this could inflict greater damage. In all cases, as compression begins and the crush is initiated, only the steel tube is in direct contact with the compression platens and creates the peak force.

4.3. Post-compression analysis

After crushing, a section from the tubes was removed to reveal the internal structure as shown in Fig. 19. From the experimental image of the auxetic strut it can be observed that where the struts had been thickened, they did not break, but rather changed orientation; whereas the thin struts did break. Consequently, the thick struts did not absorb the optimum energy.

Whilst the deformation patterns of the re-entrant and honeycomb lattice structures are relatively similar. It can be seen that the struts have clearly broken in each, highlighting the importance of wall thickness in the lattice design. The auxetic strut lattice geometry was evidently the stiffest of the three lattices, however, this did not result in the greatest energy absorption. By breaking the struts more energy was absorbed, as presented in Fig. 18.

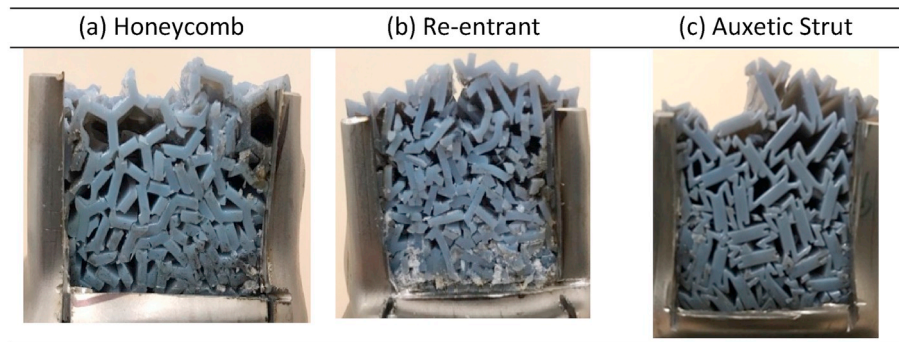


Fig. 19. Deformation of lattices after crushing.

5. Conclusions

Currently the majority of researchers are studying the effect of filling crash tubes with conventional foam or lattice structures. Auxetic foam and lattice structures have only received limited attention despite their advantageous properties. Therefore, more investigations need to be conducted to understand the full potential of such materials. In this study, the crashworthiness performance of thin-walled tubes filled with various auxetic and conventional lattices under quasi-static compressive loading is investigated. For that purpose, auxetic lattice (auxetic strut and re-entrant) filled tubes have been compared to a non-auxetic (honeycomb) filled alternative and an empty tube. Through the development of an FE computational model and experimental validation tests, it was observed that the addition of lattice structures greatly improved the crashworthiness performance of the crash tube compared with an empty tube. For example, by comparing the experimental values of energy absorption (EA), through the inclusion of a filler lattice a 62.6%, 64.0% and 79.1% increase over the empty tube were obtained for the auxetic strut, re-entrant and honeycomb structures, respectively. This corresponds to a 16.4%, 17.4% and 28.9% increase in SEA. The energy absorption characteristics of the honeycomb lattice filled crash tubes are superior to the auxetic geometries studied in this investigation. The reason for this, all structural lattices within this study were designed to be of equal mass, and as a result, the three different unit cells have different wall thicknesses. The honeycomb (hexagonal) structures have the largest thickness of 1.77 mm and so provide additional stiffness in the direction of loading.

In summary, for the selected geometries, the initial findings from placing an auxetic lattice structure inside a square crash tube are less advantageous than using a conventional honeycomb structure. However, by optimising the geometry further it is believed that the properties of auxetics can be exploited. A parametric optimisation study on the lattices, changing the parameters shown in Table 2 (i.e. h , l , t , s and θ) could achieve this.

Moreover, the crashworthiness performance of a thin-walled tubes filled with auxetic structures under oblique and lateral impact conditions can be studied. Future studies may be devoted to these subjects.

Declaration of competing interest

The authors declared that they have no conflicts of interest to this work.

CRediT authorship contribution statement

Jonathan Simpson: Investigation, Data curation, Software, Visualization, Validation, Writing - original draft. **Zafer Kazancı:** Conceptualization, Methodology, Supervision, Writing - review & editing.

Appendix A. Supplementary data

Supplementary data to this article can be found online at <https://doi.org/10.1016/j.tws.2020.106676>.

References

- [1] A. Baroutaji, M. Sajjia, A.-G. Olabi, On the crashworthiness performance of thin-walled energy absorbers: recent advances and future developments, *Thin-Walled Struct.* 118 (2017) 137–163, <https://doi.org/10.1016/j.tws.2017.05.018>.
- [2] A.A. Alghamdi, Collapsible impact energy absorbers: an overview, *Thin-Walled Struct.* 39 (2001) 189–213, [https://doi.org/10.1016/S0263-8231\(00\)00048-3](https://doi.org/10.1016/S0263-8231(00)00048-3).
- [3] W. Abramowicz, Thin-walled structures as impact energy absorbers, *Thin-Walled Struct.* 41 (2003) 91–107, [https://doi.org/10.1016/S0263-8231\(02\)00082-4](https://doi.org/10.1016/S0263-8231(02)00082-4).
- [4] A.G. Olabi, E. Morris, M.S.J. Hashmi, Metallic tube type energy absorbers: a synopsis, *Thin-Walled Struct.* 45 (2007) 706–726, <https://doi.org/10.1016/J.TWS.2007.05.003>.
- [5] S. Yuen, G.N. Nurick, The energy-absorbing characteristics of tubular structures with geometric and material modifications: an overview, *ASME. Appl. Mech. Rev.* 61 (2) (2008), <https://doi.org/10.1115/1.2885138>, 020802-020802-15.
- [6] N. Jones, *Structural Impact*, second ed. ed., Cambridge University Press, 2012.
- [7] F. Tarlochan, F. Samer, A.M.S. Hamouda, S. Ramesh, K. Khalid, Design of thin wall structures for energy absorption applications: enhancement of crashworthiness due to axial and oblique impact forces, *Thin-Walled Struct.* 71 (2013) 7–17.
- [8] M. Langseth, O.S. Hopperstad, T. Berstad, Crashworthiness of aluminium extrusions: validation of numerical simulation, effect of mass ratio and impact velocity, *Int. J. Impact Eng.* 22 (1999) 829–854.
- [9] M. Costas, J. Díaz, L. Romera, S. Hernández, A multi-objective surrogate-based optimization of the crashworthiness of a hybrid impact absorber, *Int. J. Mech. Sci.* 88 (2014) 46–54.
- [10] F. Usta, H.S. Türkmen, Experimental and numerical investigation of impact behavior of nested tubes with and without honeycomb filler, *Thin-Walled Struct.* 143 (2019), 106256, <https://doi.org/10.1016/j.tws.2019.106256>.
- [11] H. Nikkha, A. Baroutaji, Z. Kazancı, A. Arjunan, Evaluation of crushing and energy absorption characteristics of bio-inspired nested structures, *Thin-Walled Struct.* 148 (2020), 106615, <https://doi.org/10.1016/j.tws.2020.106615>.
- [12] W. Abramowicz, N. Jones, Dynamic axial crushing of square tubes, *Int. J. Impact Eng.* 2 (2) (1984) 179–208.
- [13] W. Abramowicz, N. Jones, Dynamic axial crushing of circular tubes, *Int. J. Impact Eng.* 2 (3) (1984) 263–281.
- [14] X. Zhang, H. Zhang, Experimental and numerical investigation on crush resistance of polygonal columns and angle elements, *Thin-Walled Struct.* 57 (2012) 25–36.
- [15] S.R. Guillow, G. Lu, R.H. Grzebieta, Quasi-static axial compression of thin-walled circular aluminium tubes, *Int. J. Mech. Sci.* 43 (2001) 2103–2123.
- [16] L. Mirferendesi, M. Salimi, S. Ziaei-Rad, Parametric study and numerical analysis of empty and foam-filled thin-walled tubes under static and dynamic loadings, *Int. J. Mech. Sci.* 50 (2008) 1042–1057.
- [17] Z. Kazancı, K.J. Bathe, Crushing and crashing of tubes with implicit time integration, *Int. J. Impact Eng.* 42 (2012) 80–88.
- [18] F. Tarlochan, F. Samer, A.M.S. Hamouda, S. Ramesh, K. Khalid, Design of thin wall structures for energy absorption applications: enhancement of crashworthiness due to axial and oblique impact forces, *Thin-Walled Struct.* 71 (2013) 7–17.
- [19] F. Usta, Z. Eren, H. Kurtaran, H.S. Türkmen, Z. Kazancı, Z. Mecitoğlu, Crashworthiness optimization of nested and concentric circular tubes using response surface methodology and genetic algorithm, *Lat. Am. J. Solid. Struct.* 15 (5) (2018) e42, <https://doi.org/10.1590/1679-78254385>.
- [20] L.N.S. Chiu, B.G. Falzon, D. Ruan, S. Xu, R.S. Thomson, B. Chen, W. Yan, Crush responses of composite cylinder under quasi-static and dynamic loading, *Compos. Struct.* 131 (2015) 90–98, <https://doi.org/10.1016/J.COMPSTRUCT.2015.04.057>.
- [21] Y. Wang, J. Feng, J. Wu, D. Hu, Effects of fiber orientation and wall thickness on energy absorption characteristics of carbon-reinforced composite tubes under different loading conditions, *Compos. Struct.* 153 (2016) 356–368, <https://doi.org/10.1016/J.COMPSTRUCT.2016.06.033>.

- [22] Y. Tong, Y. Xu, Improvement of crash energy absorption of 2D braided composite tubes through an innovative chamfer external triggers, *Int. J. Impact Eng.* 111 (2018) 11–20, <https://doi.org/10.1016/j.ijimpeng.2017.08.002>.
- [23] S. Santosa, T. Wierzbicki, Crash behavior of box columns filled with aluminium honeycomb or foam, *Comput. Struct.* 68 (1998) 343–367.
- [24] K.E. Evans, Auxetic Polymers: a new range of materials, *Endeavour* 15 (4) (1991) 170–174.
- [25] A.E.H. Love, *A Treatise on the Mathematical Theory of Elasticity*, New York Dover Publications, London, 1944.
- [26] R.S. Lakes, Foam structures with a negative Poisson's ratio, *Science* 235 (4792) (1987) 1038–1040.
- [27] S. Mohsenizadeh, R. Alipour, M. Shokri Rad, A. Farokhi Nejad, Z. Ahmad, Crashworthiness assessment of auxetic foam-filled tube under quasi-static axial loading, *Mater. Des.* 88 (2015) 258–268, <https://doi.org/10.1016/j.matdes.2015.08.152>.
- [28] S. Mohsenizadeh, R. Alipour, A.F. Nejad, M.S. Rad, Z. Ahmad, Experimental investigation on energy absorption of auxetic foam-filled thin-walled square tubes under quasi-static loading, *Procedia Manuf.* 2 (2015) 331–336, <https://doi.org/10.1016/j.promfg.2015.07.058>.
- [29] F. Usta, O. Ertaş, A. Ataalp, H.S. Türkmen, Z. Kazancı, F. Scarpa, Impact behavior of triggered and non-triggered crash tubes with auxetic lattices, *Multiscale Multidis. Model. Exp. Des.* 2 (2019) 119–127, <https://doi.org/10.1007/s41939-018-00040-z>.
- [30] K. Günaydin, Z. Eren, F. Scarpa, Experimental investigation of auxetic structures subjected to quasi static axial load, in: 2017 8th International Conference on Recent Advances in Space Technologies, RAST, Istanbul, 2017, pp. 7–10, <https://doi.org/10.1109/RAST.2017.8002986>.
- [31] K. Günaydin, Z. Eren, Z. Kazancı, F. Scarpa, A.M. Grande, H.S. Türkmen, In-plane compression behavior of anti-tetrachiral and Re-entrant lattices, *Smart Mater. Struct.* 28 (11) (2019) 1–14, <https://doi.org/10.1088/1361-665X/ab47c9> [115028].
- [32] T. Tancogne-Dejean, A.B. Spierings, D. Mohr, Additively-manufactured metallic micro-lattice materials for high specific energy absorption under static and dynamic loading, *Acta Mater.* 116 (2016) 14–28, <https://doi.org/10.1016/J.ACTAMAT.2016.05.054>.
- [33] K. Günaydin, Z. Eren, H.S. Türkmen, Z. Kazancı, F. Scarpa, Axial low velocity impact response of anisotropic anti-tetrachiral filling lattices, in: 7th International Conference on Mechanics and Materials in Design, 7th International Conference on Mechanics and Materials in Design-M2d2017, Algarve, Portugal, 2017, 11/06/2017.
- [34] L. Jiang, B. Gu, H. Hu, Auxetic composite made with multilayer orthogonal structural reinforcement, *Compos. Struct.* 135 (2016) 23–29.
- [35] K.L. Alderson, A.P. Pickles, P.J. Neale, K.E. Evans, Auxetic polyethylene: the effect of a negative Poisson's ratio on hardness, *Acta Metall. Mater.* 42 (7) (1994) 2261–2266.
- [36] F. Scarpa, J.R. Yates, L.G. Ciffo, S. Patsias, Dynamic crushing of auxetic open-cell polyurethane foam, *J. Mech. Eng. Sci.* 216 (2002) 1153–1156.
- [37] The British Standards Institution, *Steel Tubes for Precision Applications - Technical Delivery Conditions - Part 5: Welded Cold Sized Square and Rectangular Tubes*, 2016. Geneva.
- [38] A. Ingrole, A. Hao, R. Liang, Design and modeling of auxetic and hybrid honeycomb structures for in-plane property enhancement, *Mater. Des.* 117 (2017) 72–83.
- [39] M. Smith, *ABAQUS/Standard User's Manual, Version 6.9*, Simulia, Providence, RI, 2009.
- [40] Stratasys Ltd, Stratasys [Online]. Available: <https://store.stratasys.com/medias/?context=bWFzdGVyfiHBkZnRhZ3N8MTEyNjk0fGFwcGxpY2F0aW9uL3BkZnxxZGZ0YWdlL2hjMy9oZGYvODg2MzU5MTY2MTU5OC5wZGZ8ODE2Mjc0ZDk0NzJjMjZiOGFmI5ZWJiOWEwZjBhMzlhNTFmOTkzYmYxZmRlMzQ4NzQ3OEA2ODM4OWUwYjUwYQ.> (Accessed 28 October 2019).
- [41] M. Seitzberger, F.G. Rammerstorfer, H.P. Degischer, R. Gradinger, Crushing of axially compressed steel tubes filled with aluminium foam, *Acta Mech.* 125 (1997) 93–105.